Monte Carlo simulation study of crystallization in rapidly supercooled one-component plasmas

Shuji Ogata

Department of Physics, University of Tokyo, Bunkyo-ku, Tokyo 113, Japan
(Received 2 January 1991; revised manuscript received 13 August 1991)

Development of solidification processes in rapidly supercooled one-component plasmas is studied by a Monte Carlo (MC) simulation method with a number of particles 1458. Evolutions of interparticle correlations and of local and extended bond-orientational orders are investigated microscopically. Layered structures emerge at prenucleation stages in the system and expedite a subsequent evolution into metastable states. The metastable states are bcc monocrystalline states with an admixture of a few defects in the form of intralayer interstitials, which differ significantly from the glassy states obtained in the previous simulations with a smaller number of particles. The role of MC periodic boundary conditions in the freezing transitions is discussed in conjunction with the number of MC particles.

I. INTRODUCTION

Solidification such as crystallization and glass transition is one of the most interesting events in the thermal evolution of a many-body system. Accumulation of the effort by many investigators notwithstanding, microscopic understanding of such a transition has remained an outstanding problem. Theoretical treatment is difficult since the transition occurs catastrophically as a result of many-body correlations; it is also not easy to trace the dynamic evolutions of the microscopic structures in a laboratory experiment.

Computer-simulation study of a simple system [1], where particles interact via binary and spherically symmetric potentials, has a long history. More than three decades ago, Monte Carlo [2] (MC) and molecular-dynamics [3] (MD) simulation methods were first applied to the hard-core systems [4]. Later these methods were extended to other cases of the potentials, such as soft core [1] and Lennard-Jones [1]. The available size of the simulations has rapidly increased as the computer capabilities developed. Simulation studies of crystallization and glass transition for these systems have contributed much to the explanation for physical properties of the solids.

The classical one-component plasma [5,6] (OCP), one of the most fundamental in simple systems, is a statistical system where N particles of a single species with charge Ze interact via Coulomb potentials in a volume V with uniform neutralizing charges. Since the Coulomb potential has no characteristic length, thermodynamic properties of the OCP with number density $n = N/V$ depend only on the Coulomb coupling parameter

$$\Gamma = \frac{(Ze)^2}{ak_B T} , \qquad (1)$$

where

$$a = \left[\frac{3}{4\pi n} \right]^{1/3} \qquad (2)$$

is the ion-sphere radius. The OCP is distinct from other simple systems in at least two respects. First, the Coulomb potential is long-ranged; hence it is necessary to assess the effects of the boundary conditions carefully. Second, no volume fluctuations exist in the OCP at a fixed value of N since the background charges are incompressible; the OCP keeps its volume constant through the process of solidification.

The OCP has been treated not only as a basic model in the statistical mechanics but as a realistic model for the dense matter in the outer crust of a neutron star [7]. The main constituent of the outer crust is iron in the density-temperature regime, $\rho_m = 10^4 - 10^9$ g cm^{-3} and $T = 10^6 - 10^8$ K; hence $\Gamma = 100 - 1000$. Electrons in the crusts are relativistically degenerate and may be regarded as forming a uniform charge background for the iron ions. Physical properties of the outer crust, such as conductivities [8] and viscoelasticity [9], are essential ingredients in the analyses of the internal structure and the evolution of the star.

The equation of state for the OCP has been investigated accurately in the fluid [10–13] and in the bcc [10–12] and fcc [14] crystalline phases mainly by the MC simulation method, including dependence on the particle number N. Comparing the Helmholtz free energies between the fluid and crystalline phases, it has been found [12,13] that the fluid OCP freezes (Wigner transition) into the bcc crystals at $\Gamma_m = 178 - 180$.

It is not clear, however, what the final state of a OCP is when a rapid quench is applied to $\Gamma > \Gamma_m$. It is instructive in these connections to compare the Madelung energies [10] of the OCP between the crystalline structures,

$$\frac{E_M}{Nk_B T} = \begin{cases} -0.895\,929\Gamma & \text{(bcc)} \\ -0.895\,874\Gamma & \text{(fcc)} \\ -0.895\,838\Gamma & \text{(hcp)} . \end{cases} \qquad (3)$$

We thus find $(E_{\text{fcc}} - E_{\text{bcc}})/N = 0.010 k_B T$ and $(E_{\text{hcp}} - E_{\text{bcc}})/N = 0.016 k_B T$ at $\Gamma = 180$; the differences are only 1–2 % of the thermal energy.

The MC simulations for rapidly quenched OCP's with

$N=432$ were performed and reported earlier in Ref. [15] (referred to as paper I). The resultant final states corresponded to glasses characterized by random polycrystalline mixtures of fcc, hcp, and bcc crystalline structures. In those glasses, we found the development of layered structures [16] over the MC cell. Emerging out of those simulations are the problems: Do the layered structures have any relation with the periodic boundary conditions? How and in what stage are the layered structures formed? Is it possible to obtain a monocrystalline state, rather than a polycrystalline state, by the MC simulation method?

To answer these problems and to apply the quenched states to the investigation of the physical properties of the neutron-star crusts, we have performed new MC simulations for rapidly supercooled OCP's with a significantly increased value of N. The periodic boundary conditions depending on N may have two kinds of effects on the solidification. Under the periodic boundary conditions, any particle must move collectively with all of its images which form a simple cubic lattice with the lattice constant $L \propto N^{1/3}$. For a smaller N, the boundary conditions may hinder the motion of particles and the resultant ordering of particles. However, if N takes on a value specific to the lattice structures, such as a bcc number $2I^3$ or a fcc number $4I^3$ (I is an integer), the boundary conditions may assist in transforming the system into the respective lattice structure; such an effect may be more efficient for a smaller N. We remark that $N=432$ in paper I is one of the bcc numbers. To examine those two effects separately, we have chosen $N=1458$, another bcc number; this number is more than three times as large as that in paper I. The resulting side length of the MC cell is $L=18.3a$.

In the present paper we report detailed analyses on the results of these newly performed simulations. We find a formation of particle layers in the prenucleation stages. Internal energies at the metastable states are very close to the bcc crystalline value. Unlike the glass structures obtained in the former simulations, we find bcc monocrystalline structures in the resultant metastable states. Preliminary results have been reported in Refs. [17] and [18].

The organization of this paper is the following: In Sec. II quenching processes are described. In Sec. III we introduce bond-orientational order parameters to monitor the development of nucleation. In Sec. IV the main results are presented. Section V is devoted to a description of a separate simulation, where a supercooled fluid state is obtained. Discussion and concluding remarks are given in Sec. VI.

II. QUENCHING PROCESSES

We perform MC simulations with the usual Metropolis algorithm [19]. First a randomly selected particle is displaced tentatively by Δr with probability $P(|\Delta r|)$; the new configuration is accepted with the probability $\exp(-\Delta U/k_B T)$, where ΔU is an increment of the internal energy between the new and the original configurations (all the cases with $\Delta U < 0$ are accepted). The procedure just described constitutes a single step in
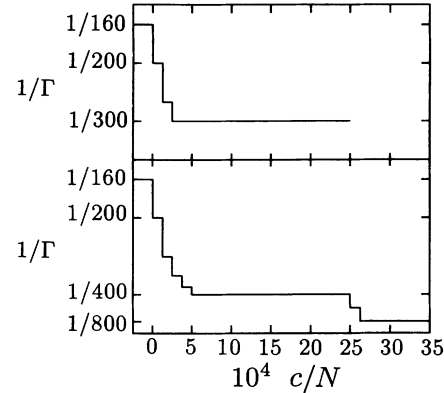

FIG. 1. Variation of $1/\Gamma$ in the MC simulation runs: (upper) is the quench to $\Gamma=300$; (lower) is the quench to $\Gamma=400$ and subsequently to $\Gamma=800$.

the MC simulations; the number of configurations so generated is denoted by c.

For the probability density of particle displacements, we have adopted a form the same as that in paper I, which is

$$P(r)=\sqrt{2\Gamma/\pi}\,\Gamma\left[\frac{r}{a}\right]^2\exp\left[-\frac{\Gamma}{2}\left[\frac{r}{a}\right]^2\right]$$ (4)

with the normalization $\int_0^\infty P(r)dr=1$. If the concept of "MC elapsed time" applies, we may estimate the elapsed time via the relation [20]

$$\omega_p t=0.12c/N \ .$$ (5)

The quenching processes are schematically depicted in Fig. 1. Starting with a fluid equilibrium state at $\Gamma=160$, we apply stepwise quenches by $\Delta\Gamma=50$ at every $c/N\times10^{-4}=1.25$, excepting for $\Delta\Gamma=40$ at $c=0$, until Γ reaches 300 [Fig. 1 (top)] and 400 [Fig. 1 (bottom)]. Phase evolution is monitored until $c/N\times10^{-4}=25.0$ in both cases. Stepwise quench to $\Gamma=800$ is applied subsequently to the final state obtained at the quench to $\Gamma=400$; simulation has been continued until $c/N\times10^{-4}=35.0$. If we assume the relation Eq. (5) for the estimation of the elapsed time, the rates of quenches to $\Gamma=300$ and 400 should be the same as those in the cases of "gradual quench" in paper I.

III. BOND-ORIENTATIONAL ORDER PARAMETERS

Orders in the particle configurations are described in terms of the orientational correlations between "bonds," which are connecting lines between a particle and its "neighboring particles." We define the neighboring particles as particles inside a sphere of radius $r/a=2.3$ around a given particle; particle positions are averaged over a sequence of $\Delta c/N\times10^{-4}=0.069$ to reduce the thermal fluctuations. The radius $r/a=2.3$ corresponds approximately to the first bottom of the radial distribution functions $g(r)$ both in the fluid phase near the freez-

ing condition shown in Fig. 2 (left) and in the bcc crystalline phase shown in Fig. 2 (right). The number N_c of neighboring particles, which we shall call the "coordination number," is 14 for the bcc cluster and 12 for the fcc, hcp, and icosahedral clusters. In the fluid simulation at $\Gamma = 160$, $N_c = 12$–14 for almost all the particles. In the bcc crystalline simulation at $\Gamma = 400$, $N_c = 14$ for all the particles. We associate a set of quantities $\{Q_{lm}(\mathbf{r})\}$ to each bond in terms of the spherical harmonics: $Q_{lm}(\mathbf{r}) = Y_{lm}[\theta(\mathbf{r}), \phi(\mathbf{r})]$, $\mathbf{r}$ is the central position of a bond, $\theta(\mathbf{r})$ and $\phi(\mathbf{r})$ are its polar angles.

The local bond-orientational order parameters [21], which are rotationally invariant combinations in the second and the third order, are introduced via

$$Q_l = \left[\frac{4\pi}{2l+1} \sum_{|m| \le l} |\langle Q_{lm}(\mathbf{r}) \rangle|^2 \right]^{1/2} , \tag{6}$$

$$W_l = \sum_{m_1 + m_2 + m_3 = 0} \begin{bmatrix} l & l & l \\ m_1 & m_2 & m_3 \end{bmatrix}$$

$$\times \frac{\bar{Q}_{lm_1}(\mathbf{r}) \bar{Q}_{lm_2}(\mathbf{r}) \bar{Q}_{lm_3}(\mathbf{r})}{\left[\sum_{|m| \le l} |\bar{Q}_{lm}(\mathbf{r})|^2 \right]^{3/2}} . \tag{7}$$

The coefficients in Eq. (7) are the Wigner $3j$ symbols [22]. The average $\bar{Q}_{lm}(\mathbf{r})$ in Eq. (7) is carried out with regard to all the bonds around a given particle; $\langle \ \rangle$ in Eq. (6) means an analogous average with respect to such bonds over all the MC particles. Quantities Q_l and W_l play the key part in the cluster "shape spectroscopy" in fluids and solids [21]. Since Q_4 assumes a first nonvanishing value (other than Q_0) in samples with cubic symmetry, and Q_6 in icosahedral systems, we take $l = 4$ and 6 in the present analyses.

The quantities (Q_4, Q_6) take on values (0.1909,0.5745) for the fcc, (0.0972,0.4848) for the hcp, (0,0.6633) for the icosahedral, and (0.0364, 0.5107) for the bcc clusters. We observe that Q_4 differs significantly from each other for the four types of clusters, while Q_6 remain almost the same. It is ascertained that (Q_4, Q_6) take on much smaller values (0.01, 0.03), in the fluid simulation at $\Gamma = 160$ than the bcc crystalline simulation values (0.04, 0.5).

The quantities W_4 and W_6 assume significantly different values between the clusters: $(W_4, W_6) = (-0.1593, -0.0132)$ for the fcc, $(0.1341, -0.0124)$ for the hcp, $(0, -0.1698)$ for the icosahedral, $(0.1593, 0.0132)$
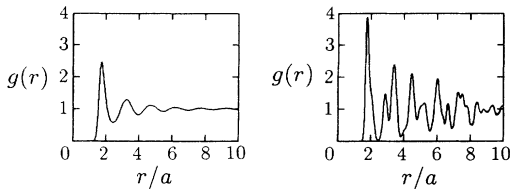

FIG. 3. Two-dimensional (W_4, W_6) maps in the fluid OCP at $\Gamma = 160$: (left) is the particles with $N_c = 12$ shown by open circles; (right) is the particles with $N_c = 14$ shown by closed circles. Diamond markers correspond to (W_4, W_6) values for the fcc, hcp, icosahedral, and bcc clusters; for the icosahedron, we set $W_4 = 0$ here.

for the bcc clusters. We remark that W_4 is not a well-defined quantity for the icosahedron since $Q_4 = 0$. The magnitude of W_6 is substantially larger for the icosahedron than for the other three types of clusters. We find that the local bond-orientational symmetries around a particle can be discerned through its location on the two-dimensional (W_4, W_6) map. Figure 3 depicts such a map for clusters with $N_c = 12$ (left) and 14 (right) at the fluid phase, and Fig. 4, for clusters with $N_c = 14$ at the bcc crystalline phase. In the fluid phase, locations of (W_4, W_6) for clusters with $N_c = 12$ and 14 scatter rather uniformly in the region $|W_4| \le 0.15$ and $|W_6| \le 0.16$. In the bcc crystalline phase, all the clusters assume $N_c = 14$. In Fig. 4 we observe that for a substantial fraction of clusters the bond-orientational parameters deviate from the bcc values, especially for the W_4 parameter owing to thermal fluctuations.

Extended bond-orientational symmetries [21] are studied in terms of the correlation functions

FIG. 2. Radial distribution functions in the fluid and bcc crystalline OCP's: (left) is the fluid simulation at $\Gamma = 160$; (right) is the bcc crystalline simulation at $\Gamma = 400$.
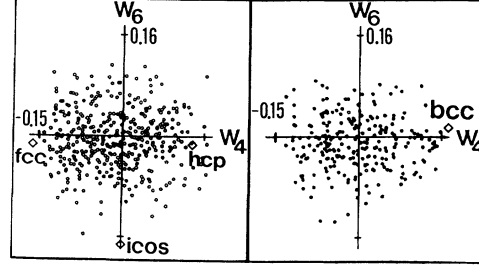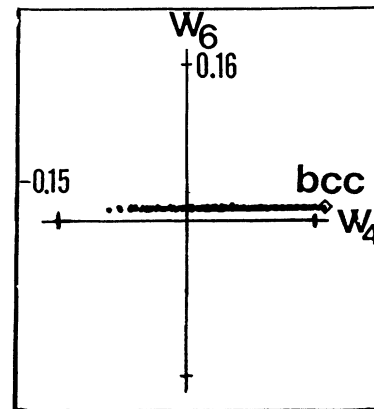

FIG. 4. Two-dimensional (W_4, W_6) map in the bcc crystalline OCP at $\Gamma = 400$ for the particles with $N_c = 14$. The diamond marker corresponds to the (W_4, W_6) value for the bcc cluster.
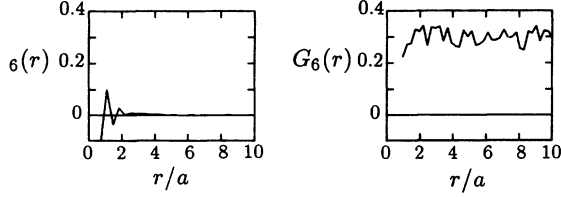
FIG. 5. Bond-orientational correlation function $G_6(r)$: (left) is the fluid simulation at $\Gamma=160$; (right) is the bcc crystalline simulation at $\Gamma=400$.

$$G_l(r) = \frac{4\pi}{(2l+1)G_0(r)} \sum_{|m|\leq l} \langle Q_{lm}(\mathbf{r})Q_{l-m}(0) \rangle , \qquad (8)$$

where $G_0(r)=4\pi\langle Q_{00}(\mathbf{r})Q_{00}(0)\rangle$. $G_l(r)$ take on first nonvanishing values at $l=6$ for the bcc structure. We find in Fig. 5 (left) that $G_6(r)\simeq 0$ in the fluid simulation at $\Gamma=160$, indicating absence of an extended order. In the bcc crystalline phase at $\Gamma=400$, $G_6(r)\simeq 0.3$ as shown in Fig. 5 (right), confirming the existence of a long-range extended order.

IV. DEVELOPMENT OF CRYSTALLIZATION

A. Excess internal energies

Excess internal energy [6] is a primary quantity in characterizing the states of OCP since its volume is fixed. Evolution of the excess internal energy per particles, averaged over a sequence of $\Delta c/N\times 10^{-4}=0.007$,

$$u \equiv \frac{U}{Nk_BT} = \left\langle \frac{n}{2k_BT} \int d\mathbf{r} \frac{(Ze)^2}{r}[\hat{g}(r)-1] \right\rangle , \qquad (9)$$
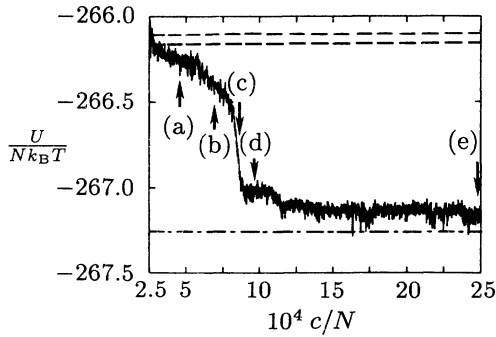
where (m is an integer vector)

FIG. 6. Evolution of the normalized excess internal energy for the quench to $\Gamma=300$. Stages are specified at (a) 4.6, (b) 7.0, (c) 8.6, (d) 9.5, and (e) 24.9. The dashed lines indicate the levels predicted from the extensions of the fluid internal-energy formulas [upper: Eq. (11); lower: Eq. (12)]; the dotted-dashed line, the bcc crystalline level via Eq. (13).

$$n\hat{g}(\mathbf{r}) = \frac{1}{N} \sum_{i=1}^{N} \left[\sum_{j\neq i} \delta(\mathbf{r}_i - \mathbf{r}_j - \mathbf{r}) \right.$$
$$\left. + \sum_{m\neq 0} \sum_{j=1}^{N} \delta(\mathbf{r}_i - \mathbf{r}_j + \mathbf{m}L - \mathbf{r}) \right] \qquad (10)$$

is shown in Fig. 6 for the quench to $\Gamma=300$ and in Fig. 7 for the quench to $\Gamma=400$.

In each figure dashed lines imply the extrapolation values of the fluid internal energy formula,

$$u = -0.897\,744\Gamma + 0.950\,43\Gamma^{1/4} + 0.189\,56\Gamma^{-1/4}$$
$$-0.814\,87 \qquad (11)$$

due to Slattery, Doolen, and DeWitt [12] for the upper line, and

$$u = -0.898\,004\Gamma + 0.967\,86\Gamma^{1/4} + 0.220\,703\Gamma^{-1/4}$$
$$-0.860\,97 \qquad (12)$$

due to Ogata and Ichimaru [13] for the lower. The dotted-dashed line means the bcc crystalline value, according to the formula [12]

$$u = -0.895\,929\Gamma + 1.5 + 322\,5\Gamma^{-2} . \qquad (13)$$

We note that the fcc crystalline value [14] of u are higher than the bcc one only by 0.01–0.02 for $\Gamma=300$–400.

In the case of the quench to $\Gamma=300$, u stays around the fluid extrapolation value for $c/N\times 10^{-4}=2.5$–6.0. It gradually decreases as c increases for $c/N\times 10^{-4}=6.0$–8.0, and decreases abruptly at $c/N\times 10^{-4}=8.0$–9.0 and at 11.0–12.0; after $c/N\times 10^{-4}\simeq 12.0$, it is metastable though jitters are observed. The evolution of u for the quench to $\Gamma=400$ is similar to that for the case with $\Gamma=300$; u stays around the fluid extrapolation for $c/N\times 10^{-4}=5.0$–7.5. It gradually decreases as c increases for $c/N\times 10^{-4}=7.5$–15.0, and decreases abruptly at $c/N\times 10^{-4}=15.0$–17.0; after $c/N\times 10^{-4}\simeq 17.0$, it is metastable. The deviations of u at the metastable states from the bcc crystalline phase are 0.08 ($\Gamma=300$) and 0.21 ($\Gamma=400$). Those are far smaller than the values 0.25 ($\Gamma=300$) and 0.4 ($\Gamma=400$) for the glassy states in paper I.

Five stages for the quench to $\Gamma=300$ are defined in Fig. 6: (a) at $c/N\times 10^{-4}=4.6$, (b) 7.0, (c) 8.6, (d) 9.5, (e)
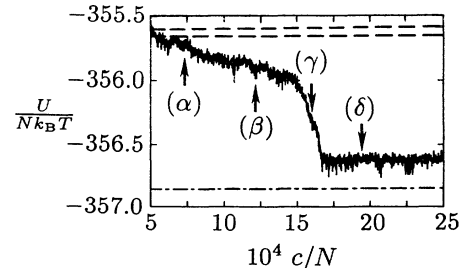

FIG. 7. Same as Fig. 6, but for the quench to $\Gamma=400$. Stages are specified at (α) 7.3, (β) 12.1, (γ) 15.8, and (δ) 19.5.

24.9. For the quench to $\Gamma=400$, four stages are also defined in Fig. 7: (α) 7.3, (β) 12.1, (γ) 15.8, (δ) 19.5. Stages (c) and (γ) correspond to a midst of the abrupt decreases in u for the quenches to $\Gamma=300$ and 400, respectively.

B. Radial distribution functions

Evolution of $g(r)=\langle g(\mathrm{r})\rangle$ averaged over $\Delta c/N\times10^{-4}=0.21$ is displayed in Fig. 8 for the quench to $\Gamma=300$, and in Fig. 9 for the quench to $\Gamma=400$. For the quenches to $\Gamma=300$ and 400, $g(r)$ exhibits a smooth feature analogous to that in a fluid simulation [see Fig. 2 (left)] at the stages before the abrupt decreases in u [(a), (b), (α), and (β)]. For the quench to $\Gamma=300$, the second and third peaks of $g(r)$ have shoulders at radii corresponding to the bcc peaks at stage (c). The system seems to have acquired a substantial degree of the bcc local

structures at stage (c). We find no substantial change in $g(r)$ from stage (c) to (d). At stage (e), $g(r)$ is quite similar to the one in the bcc crystalline simulation [see Fig. 2 (right)]. Though positions and heights of the peaks in $g(r)$ at stage (e) resemble those in the bcc crystalline simulation, we find a clear difference at the first bottom of $g(r)$; finiteness of $g(r)$ at the first bottom indicates a deviation from the bcc crystalline structures [see Fig. 2 (right)]. For the quench to $\Gamma=400$, $g(r)$ retains a smooth feature at the stage (γ), though u decreases abruptly at this stage. Stage (γ) may be considered as an initial stage for the transition to the local bcc structures. Some degrees of deviation from the bcc crystalline structures still exist at the stage (δ) since the first bottom of $g(r)$ takes on a nonvanishing value.

Features of $g(r)$ for the metastable states in both quenches are quite different from those for the simulations with $N=432$. We found no peaks corresponding to the bcc structures in all the cases of the quench with $N=432$. In one case, a few peaks appeared at the radii corresponding to the fcc-hcp structures. In other cases, however, we found several little peaks at those radii which have no correspondence to the fcc-hcp and bcc structures.
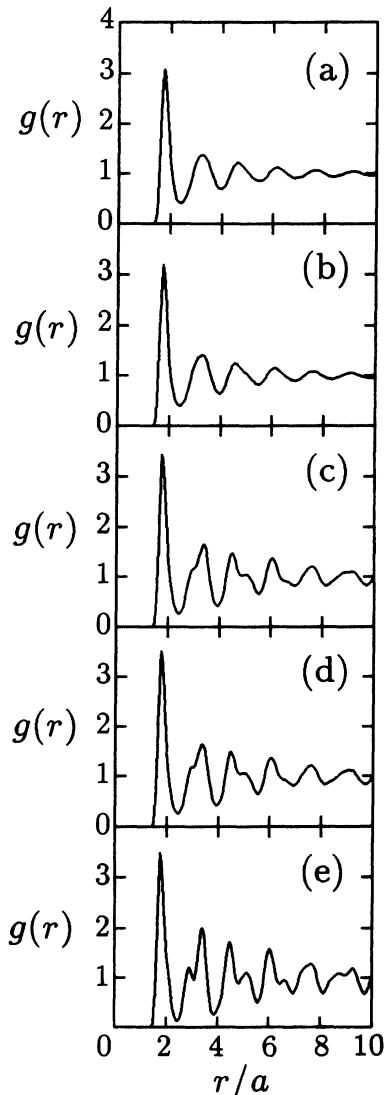

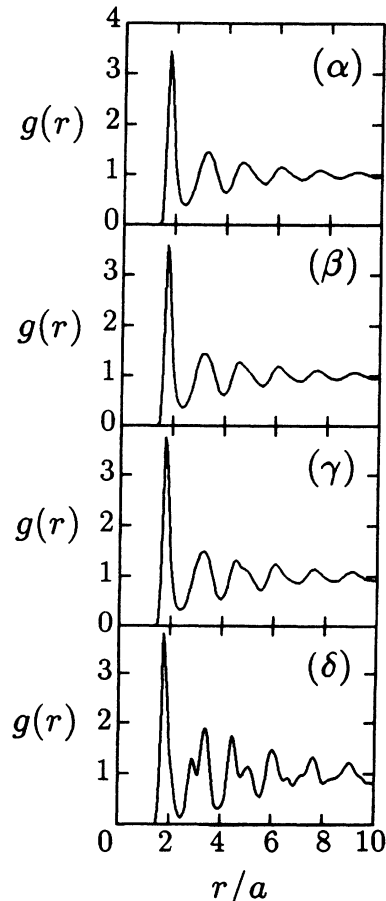FIG. 8. Evolution of the radial distribution function for the quench to $\Gamma=300$.

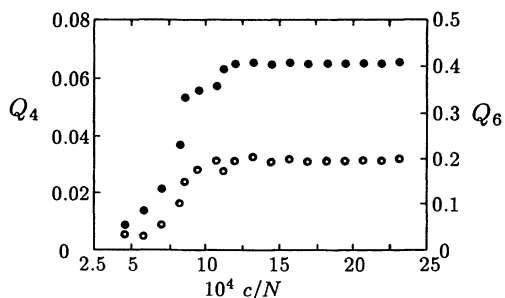FIG. 9. Same as Fig. 8, but for the quench to $\Gamma=400$.

FIG. 10. Evolution of the bond-orientational parameters Q_4 and Q_6 for the quench to $\Gamma = 300$. Open circles correspond to Q_4 values; closed circles, Q_6 values.

FIG. 12. Evolution of the fractional numbers of particles with various N_c for the quench to $\Gamma = 300$: open circles, those with $N_c = 12$; crosses, those with $N_c = 13$; and closed circles, those with $N_c = 14$.

C. Local bond-orientational orders

Evolutions of the local bond-orientational order parameters (Q_4, Q_6) are depicted in Fig. 10 for the quench to $\Gamma = 300$ and in Fig. 11 for the quench to $\Gamma = 400$. For the quench to $\Gamma = 300$, the rate of increase in Q_6 steepens at $c/N \times 10^{-4} = 6.0$–7.0, followed by the first abrupt decrease in u at $c/N \times 10^{-4} = 8.0$–9.0. At the second abrupt decrease in u around $c/N \times 10^{-4} = 11.0$–$12.0$, Q_6 increases stepwise to $Q_6 \simeq 0.41$. In regard to Q_4, we find its increase at one time, $c/N \times 10^{-4} = 8.0$–9.0, corresponding to the first decrease in u; thereafter, $Q_4 \simeq 0.035$. For the quench to $\Gamma = 400$, both Q_4 and Q_6 increase concurrently with the decrease in u. Q_6 reaches 0.45 after its abrupt increase at about $c/N \times 10^{-4} = 15.0$–$17.0$. Also for the quantity Q_4, it jumps up to 0.039 at $c/N \times 10^{-4} = 15.0$–$16.0$. Final values of (Q_4, Q_6) in both quenches are approximately the bcc values (see Sec. III). The aforementioned difference in the evolutional processes of Q_6 between the two quenches indicates that the local orders in the two quenches develop in different ways.

We have thus found that the metastable states have a long-ranged bond-orientational order extending over the entire MC cell at the same level as that in a bcc crystalline state. Comparing the evolution of Q_4 with that of Q_6 in both quenches, we might remark that Q_4 is a parameter insensitive to the freezing in OCP's; this may be connected with the fact that $Q_4 = 0$ for icosahedron, one of the close-packing structures.

Since the values of N_c differ between clusters, it would be instructive to look into the evolutions in the fractional
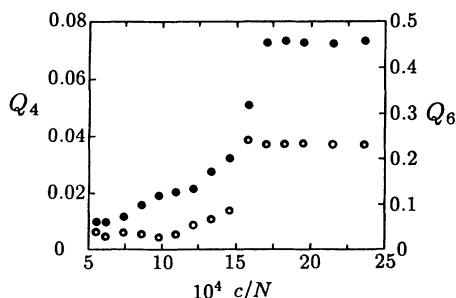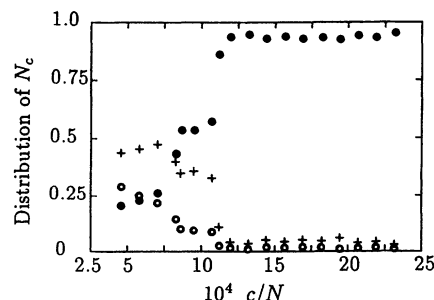
numbers of the particles with $N_c = 12$, 13, and 14 in Fig. 12 for the quench to $\Gamma = 300$ and in Fig. 13 for the quench to $\Gamma = 400$. For the fluid state at $\Gamma = 160$, the fractional numbers are 0.30, 0.45, 0.20 for $N_c = 12,13,14$, respectively. For both cases of quenches, the fractional number with $N_c = 14$ increases at the stages where u decrease abruptly. Finally, about 95% of clusters in the metastable state have $N_c = 14$ for the quench to $\Gamma = 300$; and about 83% for the quench to $\Gamma = 400$. These fractional numbers for $N_c = 14$ in both quenches are much larger than the values 10–50 % in the cases with $N = 432$.

Evolutions of the two-dimensional (W_4, W_6) maps for clusters with $N_c = 12$ and 14 are plotted in Fig. 14 for the quench to $\Gamma = 300$ and in Fig. 15 for the quench to $\Gamma = 400$. In the figures, the (W_4, W_6) values for the reference clusters are likewise displayed by the diamond markers.

For the quench to $\Gamma = 300$, (W_4, W_6) values are distributed almost uniformly in the region $|W_4| \leq 0.15$ and $|W_6| \leq 0.16$ at stages (a) and (b); this is a typical behavior in a fluid (see Fig. 3). We find that substantial proportion of clusters with $N_c = 14$ has local bcc symmetry at stage (c); distribution of these clusters resembles that of the bcc crystalline simulation (see Fig. 4). We may interpret several subpeaks of $g(r)$ at radii corresponding to the bcc peak positions at stage (c); a certain degree of local bcc symmetry is manifested. At stage (d), distribution of
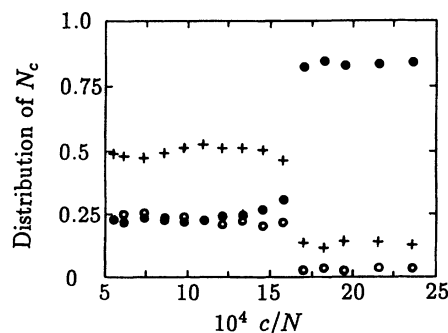

FIG. 11. Same as Fig. 10, but for the quench to $\Gamma = 400$.

FIG. 13. Same as Fig. 12, but for the quench to $\Gamma = 400$.

clusters with $N_c = 14$ is centered at around $W_6 \simeq 0.013$, the bcc value, concurrent with the decrease in number of clusters with $N_c = 12$. At a subsequent stage (e), we observe an increased degree of local bcc symmetry in the distribution of clusters with $N_c = 14$.

For the quench to $\Gamma = 400$, distributions of clusters with $N_c = 12$ and 14 at stages (α) and (β) resemble those for the fluid phase. At stage (γ), some fractions of clusters with $N_c = 12$ coalesce at the fcc marker; at this stage, a concentration to $W_6 \simeq 0.013$ takes place for clusters with $N_c = 14$. The smooth feature of $g(r)$ observed at stage (γ) may be attributed to such a coexistence of the local fcc and bcc symmetries. At stage (δ), only a small

number of clusters with $N_c = 12$, which have no fcc or hcp structures remaining, and clusters with $N_c = 14$ have the bcc symmetry to a large extent.

All the analyses on the local orders mentioned above consistently show that the metastable states in both quenches have almost perfect local bcc structures. The metastable states in the present quenches, therefore, have local structures quite different from the mixture of local fcc, hcp, and bcc structures for the glass states obtained in paper I.

D. Extended bond-orientational orders

Evolution of the extended bond-orientational symmetries are displayed in terms of $G_6(r)$ in Fig. 16 for the quench to $\Gamma = 300$ and in Fig. 17 for the quench to $\Gamma = 400$. For the quench to $\Gamma = 300$, no extended order exists at stage (a). At stage (b), bond correlations extend themselves approximately two-thirds of L. At stage (c), $G_6(r) \simeq 0.1$ in the entire MC cell; hence, the system exhibits a degree of long-range order. For the quench to $\Gamma = 400$, $G_6(r)$ is short-ranged at stage (α). At stage (β) bond-correlation length extends to a half of L. Bond-orientational correlation becomes long-ranged at the stage (γ) to the same degree as with stage (c) for the
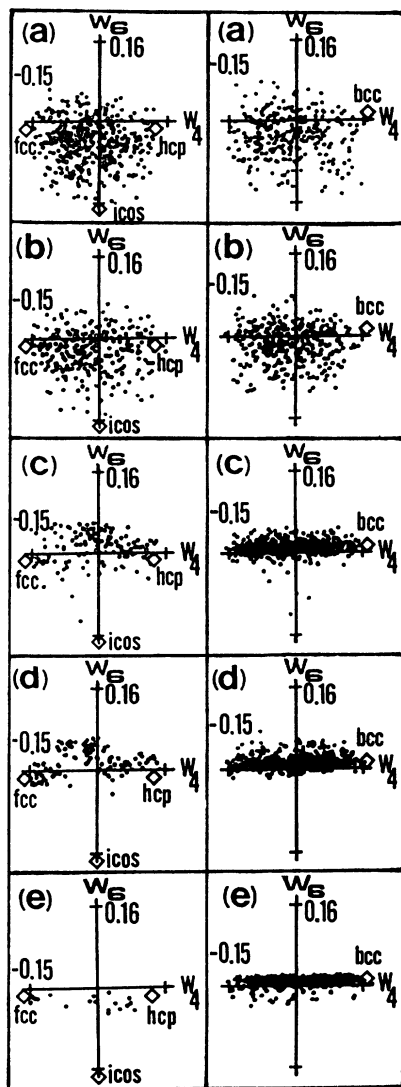

FIG. 14. Evolution of two-dimensional (W_4, W_6) maps for the quench to $\Gamma = 300$: (left) is the particles with $N_c = 12$ shown by open circles; (right) is the particles with $N_c = 14$ shown by closed circles. Diamond markers correspond to (W_4, W_6) values for the fcc, hcp, icosahedral ($=$icos), and bcc clusters; for the icosahedron, we set $W_4 = 0$ here.
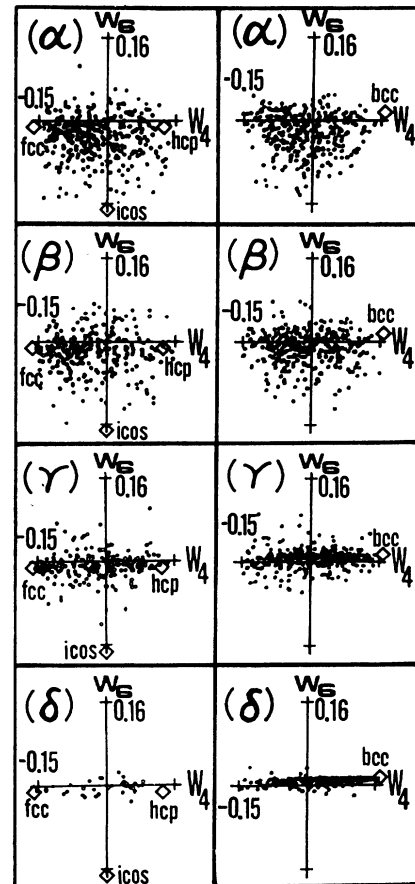

FIG. 15. Same as Fig. 14, but for the quench to $\Gamma = 400$.

quench to $\Gamma = 300$. Final values of $G_6(r)$ in both quenches are about two-thirds of the bcc value.

E. Layered structures

One of the main concerns in the present simulations has been a possible formation of the layered structures and their relation to the periodic boundary conditions. For elucidation of such an issue, two-dimensional projection maps of particles have been constructed from various directions to illustrate possible layered structures. We begin isolating those particles inside a sphere of radius $L/2$, then rotating these as a whole by an angle ζ around the y axis and by η around the z axis; the resulting configuration is projected onto the y-z plane. (Note that the particle positions are averaged over a sequence of $\Delta c /N \times 10^{-4} = 0.069$.) For each of the stages (a)–(e) and (α)–(δ), we have thus constructed maps from various an-
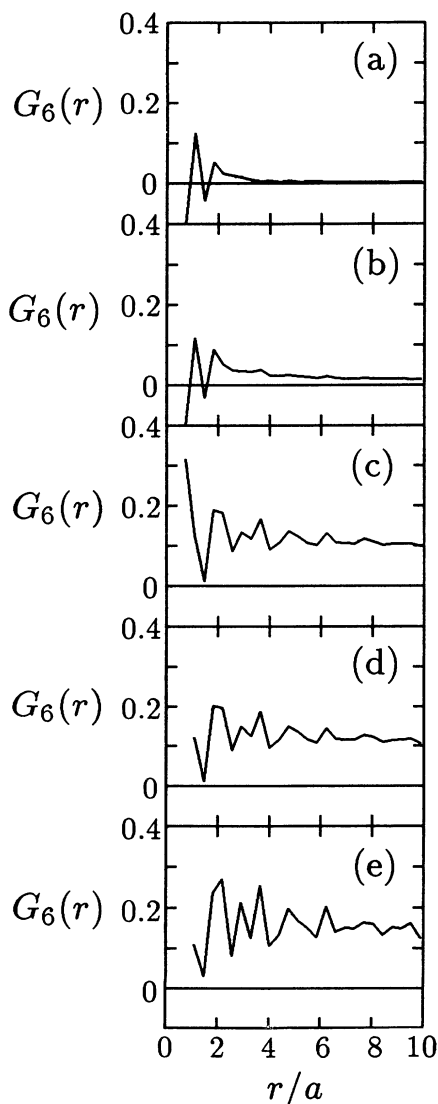

FIG. 16. Evolution of bond-orientational correlation function $G_6(r)$ for the quench to $\Gamma = 300$.
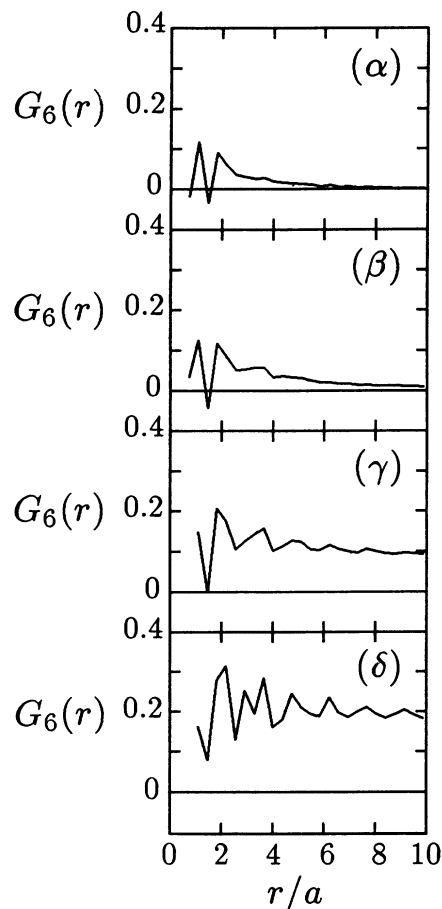

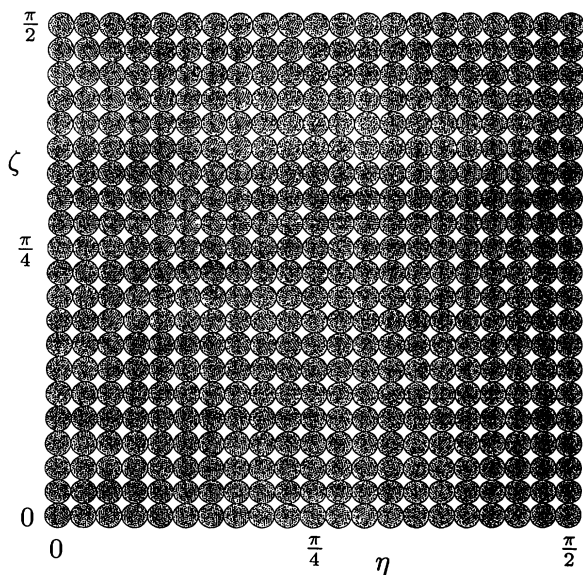FIG. 17. Same as Fig. 16, but for the quench to $\Gamma = 400$.

FIG. 18. A collection of maps which are made by projecting particles onto the y-z plane with various rotation angles $(\zeta,\eta) = [(\pi/40)i,(\pi/40)j]$, $i,j = 0,1,...,20$.

gles $(\zeta,\eta)=[(\pi/40)i,(\pi/40)j]$ with $i,j=0,1,...,20$.

Such a collection of maps at a prenucleation stage (α) for the quench to $\Gamma=400$ is shown in Fig. 18. We find particles forming a layer like structure in the map with $(\zeta,\eta)=(11\pi/40,2\pi/5)$. Also at stage (a) for the quench to $\Gamma=300$, we find layered structures emerging at different angles $(\zeta,\eta)=(\pi/4,\pi/5)$ from those for the quench to $\Gamma=300$.

Evolutions of such particle layers are depicted in Fig. 19 for the quench to $\Gamma=300$ viewed at the same angles $(\zeta,\eta)=(\pi/4,\pi/5)$ and in Fig. 20 at $(\zeta,\eta)=(11\pi/40,2\pi/5)$ for the quench to $\Gamma=400$. Particle

layers develop over a half of the sphere at stages (b) and (β). We find nearly perfect layers already at stage (c) for the quench to $\Gamma=300$. For the quench to $\Gamma=400$, we find two domains at stage (γ): in one domain, particles are well-ordered forming nearly perfect layers; in the other domain, particles show a rather disordered feature. At stage (δ), the domain of well-ordered particles spread over the cell. Such an emergence of two domains at stage (γ) may be understood as a result of the coexistence of local fcc and bcc symmetries seen in Fig. 15.

If the formation of layered structures has anything to do with the periodic boundary conditions in the cell, orientations of emerged layers would have a cubic symmetry. We single out the two cases where the layered structures are found at the prenucleation stages. The two values of the angle ζ are very close to each other and approximately take on $\pi/4$, half the characteristic angle for the cubic symmetry. On the other hand, the values of the angle η in both cases are multiples of $\pi/5$, characteristic angles for the fivefold symmetry. Further investigation on the relation between the periodic boundary condition
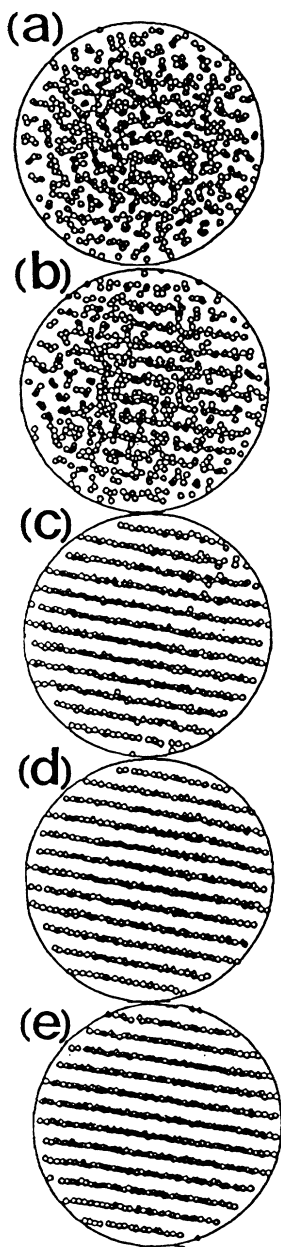

FIG. 19. Evolution of layered structures for the quench to $\Gamma=300$ viewed at angles $(\zeta,\eta)=(\pi/4,\pi/5)$.
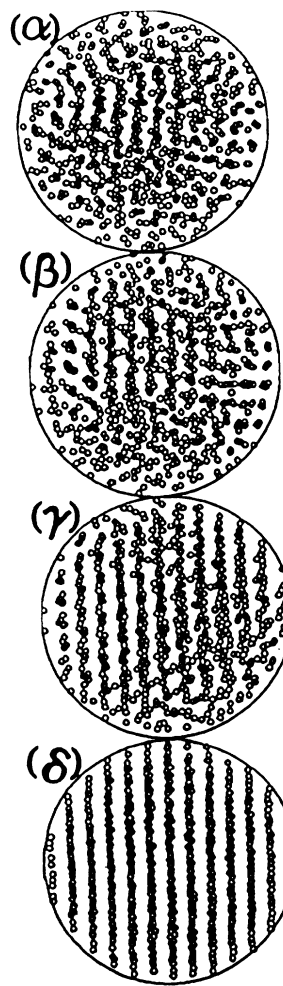

FIG. 20. Same as Fig. 19, but for the quench to $\Gamma=400$ at angles $(\zeta,\eta)=(11\pi/40,2\pi/5)$.
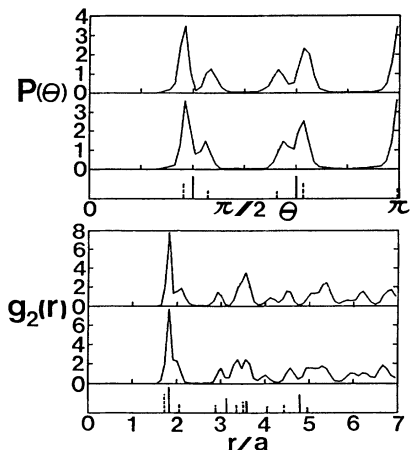
FIG. 21. Bond-angle distribution $P(\theta)$ and two-dimensional radial distribution function $g_2(r)$ between intralayer particles in stages (e) (upper) and (δ) (lower). The bottom figures show the corresponding quantity for the bcc (dashed lines) and for the fcc, i.e., hexagonal, (solid lines) lattices.

and the emergence of layered structures in a prenucleation stage would require an increased number of samples.

In the metastable states for the quenches with $N=432$, we found layers at angles $(\zeta,\eta)=(\pi/20,\pi/2)$, $(3\pi/20,0)$, and $(17\pi/40,\pi/40)$. In these cases, we could not detect such an indication of possible cubic symmetry.

Since all the particles reside on layers at the final stages (e) and (δ) as in the case of a lattice structure, two-dimensional particle positions on the layers may contain some imperfections. We investigate the character of the final states, (e) and (δ), from the point of view of intralayer correlations by the two-dimensional radial distribution function $g_2(r)$, and the correlation of bond angles $P(\theta)$ around a particle. Here, bonds are redefined as the connecting lines between a particle and its neighboring particles on a layer inside the circle of radius $2.5a$, which correspond approximately to the first minimum of $g_2(r)$. We note that about 97% of the particles have six particles inside a circle of $r/a=2.5$ at stages (e) and (δ).

Figure 21 shows $g_2(r)$ and $P(\theta)$ at stages (e) (upper) and (δ) (lower). At the bottom of the figure, intralayer correlations on the most closely packed planes for each structure are shown: vertical solid lines depict the correlations for the fcc-hcp hexagonal planes; vertical dashed lines for the bcc $\{110\}$ planes. Peak positions and heights of $g_2(r)$ and $P(\theta)$ are nearly identical to the bcc structures. Nevertheless, we find substantial degrees of deviation from the bcc structures: for instance, $P(\theta)$ around $\theta \sim \pi/2$ and $g_2(r)$ around $r \sim 2.5a$ do not vanish. Both for stages (e) and (δ), imperfections are found in the particle correlations on the layers.

F. Motion of defects

Since u shows transient behaviors in the metastable region, it appears probable that the final state may trans-

form into a purely bcc crystalline state by a further extension of the MC samplings. To estimate the probability of such a transition, we investigate the character of the intralayer imperfections and their dynamics during the metastable state by tracing the motion of particles.

The following three periods are defined in terms of $c/N \times 10^{-4}$: (1) 12.6–16.7, (2) 16.7–20.8, (3) 20.8–24.9. In each of the three periods, we first single out particles in a layer (exemplified in Figs. 19 and 20) that extends continuously into the surrounding image cells at the final configuration, and projects these (solid circles) on the x-z plane. Then their positions are traced back to the begin-
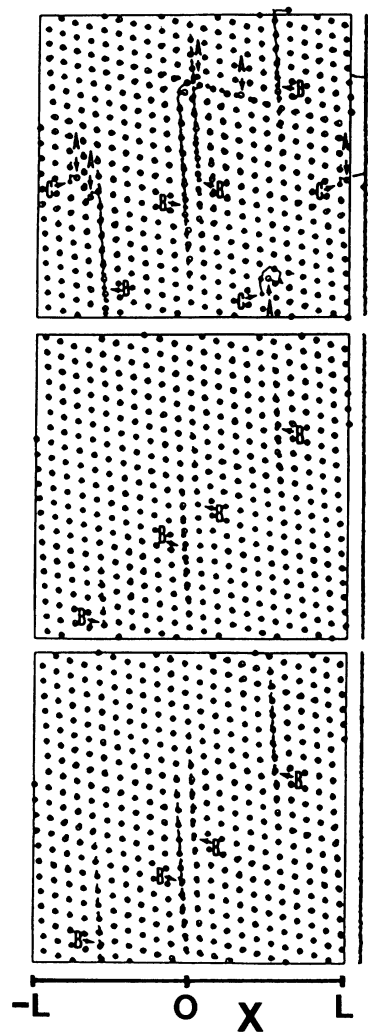

FIG. 22. Motions of particles in and near a layer (size: $2L \times 2L$) projected onto a x-z plane for the quench to $\Gamma = 300$ during the periods $c/N \times 10^{-4} = 12.6$–$16.7$ (top), 16.7–20.8 (middle), and 20.8–24.9 (bottom). The open circles denote the positions at the beginning of a period, the solid circles, those at the end; in between 19 particle positions follow at an equal interval of $\Delta c/N \times 10^{-4} = 0.21$. Examples of type (A), (B), and (C) imperfections are shown. The pairs of vertical noisy lines (left for $x < 0$, right for $x > 0$) depict the projections of the particle motions onto a y-z plane.

ning of the period (open circles) with an equal interval of $\Delta c/N \times 10^{-4} = 0.21$. Such maps, extended to the size $2L \times 2L$ to see the linked motion of particles, are depicted in Fig. 22 for the quench to $\Gamma = 300$: (top) corresponds to period (1); (middle), for the same layer as the top, but to period (2); (bottom), for the same layer as the top, but to period (3). The pairs of vertical noisy lines depict the projections of the particle positions during the corresponding period on a $y - z$ plane: the left line is for $x < 0$ particles; the right, for $x > 0$ particles. For the quench to $\Gamma = 400$, we depict in Fig. 23 such a map for period (3).

The imperfections found in these analyses can be classified into three types: (A) a particle outside the layer (belonging mostly to one of the adjacent layers) in the open-circle configurations, (B) an interstitial (or an extra particle outside the adjacent layers) in the layer, and (C) a vacancy in the open-circle configurations. For the quench to $\Gamma = 300$, we find real transitions during period (1) (top of Fig. 22) in the forms of merges between (A) and (C) and between (B) and (C) and of a transformation (or a settling) from (A) to (B), as well as virtual transitions within (B); the virtual transition usually ceases at a return to the original interstitial configurations. We attribute these real transitions as the causes of the transient behaviors of u around $c/N \times 10^{-4} = 14.0$. During periods (2) and (3) (middle and bottom of Fig. 22), however, no imperfections of the types (A) and (C) appear to remain in the system; transient behaviors in u arise only through the virtual transitions within (B). For the quench to $\Gamma = 400$ (Fig. 23), we find only virtual transitions within type-(B) imperfections in period (3). The jitters observed in the metastable states shown in Figs. 6 and 7 are attributed to those incidents of the virtual transitions.

We thus characterize the imperfections at the final states in both quenches as intralayer interstitials. An annihilation of such an isolated interstitial by the MC sampling processes would call for a slight but homogeneous compression of a configuration of particles that surround the interstitial in the layer, concurrent with appropriate compressions of the particle configurations in the neighboring layers, in such a way as to preserve the overall bcc
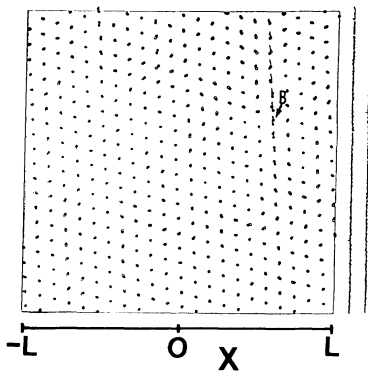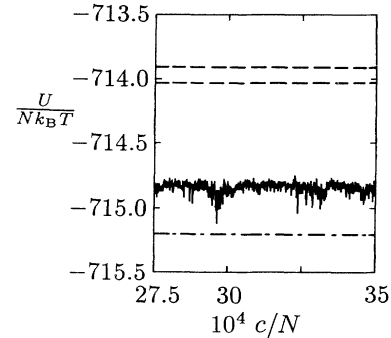

FIG. 24. Same as Fig. 6, but for the further quench to $\Gamma = 800$.

crystalline structures. We speculate the probability of such a sampling, if not zero, would be extremely small.

G. Quench to $\Gamma = 800$

One expects the possibility that a further increase in Γ might introduce some additional changes to the final state since the deviation of Madelung energy in units of $k_B T$ from the purely bcc crystalline state grows proportional to Γ. Besides, a state where the Γ parameter is as large as 1000 may become necessary when application of the MC results is considered in the outer crustal matter of the neutron stars. We therefore perform an additional MC simulation for a further quench. Starting from the final state for the quench to $\Gamma = 400$ (i.e., at $c/N \times 10^{-4} = 25.0$), we increase Γ stepwise through 600 to 800, and maintain it until $c/N \times 10^{-4} = 35.0$ as shown in Fig. 1 (bottom).

Excess internal energies u, depicted in Fig. 24, stay about 0.2 above the bcc value (dashed line), though transient behaviors are seen at around $c/N \times 10^{-4} = 28.5$ and 33.0. No change in $g(r)$ is observed during the run after the quench to $\Gamma = 800$. Figure 25 shows such a $g(r)$ at $c/N \times 10^{-4} = 32.4$. In Fig. 26, motion of particles in the same layer as in Fig. 23 is described on a x-z plane from open circles to solid circles during the period $c/N \times 10^{-4} = 30.7$–34.8 with an equal interval of

FIG. 23. Same as Fig. 22, but for the quench to $\Gamma = 400$ during the period $c/N \times 10^{-4} = 20.8$–24.9. An example of type-(B) imperfection is shown.
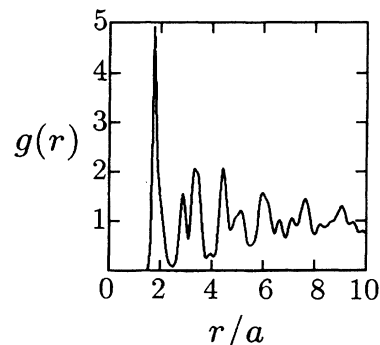

FIG. 25. The radial distribution function at $c/N \times 10^{-4} = 32.4$ for the further quench to $\Gamma = 800$.
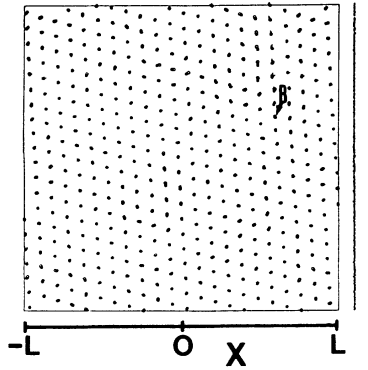
FIG. 26. Same as Fig. 22, but for the further quench to $\Gamma = 800$ during the period $c/N \times 10^{-4} = 30.7 - 34.8$. The same layer is chosen as in Fig. 23.

FIG. 28. Same as Fig. 25, but at $c/N \times 10^{-4} = 7.2$ for the quench to $\Gamma = 200$.

$\Delta c/N \times 10^{-4} = 0.21$. A pair of vertical noisy lines depict the projections of the particle positions onto a y-z plane: the left line is for $x < 0$ particles; the right, for $x > 0$ particles. We find that motions of particles are locked around their original positions.

It has not been possible to remove the defects produced during the rapid quenches through application of a further quench to the system.

V. SUPERCOOLED FLUID STATE

The OCP has the lowest free energies for the bcc phase at $\Gamma > \Gamma_m = 180$. MC simulations with $N \leq 1024$, however, indicate that the supercooled fluid OCP at $\Gamma = 200$ appears stable. The stability of the OCP in the supercooled fluid state would be attributed to a limited span of simulations and to the periodic boundary conditions. We study the stability of the supercooled fluid OCP with $N = 1458$ by performing an additional long run. Starting with the fluid state at $\Gamma = 160$, we apply a sudden quench to $\Gamma = 200$ at $c = 0$. The evolution is monitored until $c/N \times 10^{-4} = 7.5$.

Figure 27 shows u as a function of c/N. u stays at the fluid extrapolation level (dashed lines) immediately after the quench to the final configuration. During $c/N \times 10^{-4} = 0.6 - 7.5$, $g(r)$ continues to exhibit a smooth
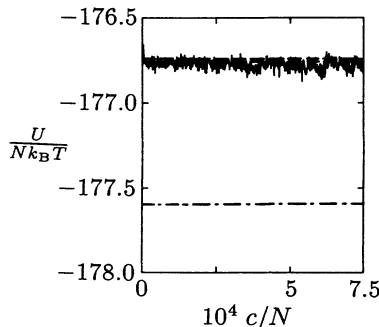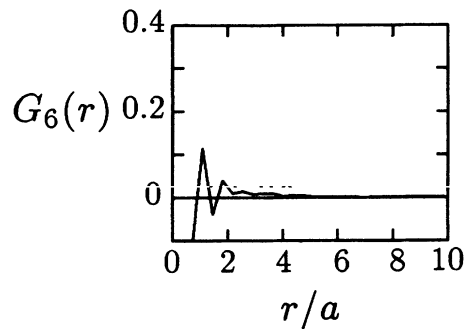

FIG. 29. Bond-orientational correlation function $G_6(r)$ at $c/N \times 10^{-4} = 7.2$ for the quench to $\Gamma = 200$.

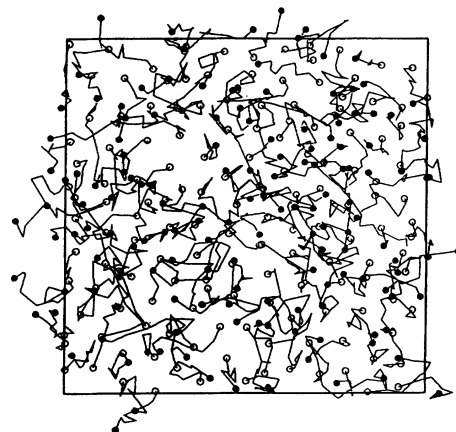FIG. 27. Same as Fig. 6, but for the quench to $\Gamma = 200$.

FIG. 30. Motion of particles inside a slab of width $\Delta z = 2.0a$ for the quench to $\Gamma = 200$ during the period $c/N \times 10^{-4} = 5.7 - 7.3$. The open circles denote the positions at the beginning of a period, the solid circles, those at the end; in between eight particle positions follow at an equal interval of $\Delta c/N \times 10^{-4} = 0.21$.

feature. Figure 28 depicts $g(r)$ at $c/N \times 10^{-4} = 7.2$, near the last configuration. Distributions of (W_4, W_6) values for clusters with $N_c = 12$ and 14 scatter as in the fluid case at $\Gamma = 160$. Bond correlation is short-ranged since $G_6(r) \simeq 0.0$ as shown in Fig. 29. Diffusive motions of particles are traced in Fig. 30 from $c/N \times 10^{-4} = 5.7$ (open circles) to 7.3 (solid circles) with an equal interval $\Delta c/N \times 10^{-4} = 0.21$ for those inside a slab of width $\Delta z = 2.0a$ at the open circle configurations. In all the analyses, we found no indications of phase transitions.

VI. DISCUSSION AND CONCLUDING REMARKS

In the present simulations, rapidly quenched OCP's have solidified into bcc monocrystalline states with defects. Microscopic structures in these final states are significantly different from those in the polycrystalline glasses obtained in the former simulations with $N=432$. Since the quenching procedures are almost the same in both simulations, the difference in the final states should be attributed to the difference in N. The choice of N at a bcc number appears to bear no essential consequences to the solidification processes since substantial numbers of imperfections from the perfect bcc crystalline states have been observed in both metastable states. By considering the effects of the periodic boundary conditions as to hinder the motion of particles for smaller N, we may explain the mechanism of the formation of the metastable states in both simulations: When the OCP is rapidly quenched to $\Gamma > \Gamma_m$, particle layers emerge first in an arbitrary direction, which would favor fcc-hcp local structures. Subsequently the system may transform itself into

a bcc crystalline state if N is large enough, since the Helmholtz free energies assume the lowest values in the bcc phase. In case that N is no large enough, however, the motion of particles would be hindered by the boundary conditions resulting in a mixture of fcc, hcp, and bcc structures; this would be the case for the simulations with $N=432$.

Emergence of layered structures preceding the nucleation may be a characteristic of the solidification processes in OCP's. Experiments [23] and computer simulations [24,25] have discovered that the charged particles in an external confining field freeze into a state in which shell (layer) structures are formed in the field direction. The long-range nature of the Coulomb force, which is a feature common to both systems, might be a cause for the emergence of a layered structure in these rapidly quenched systems.

In the present simulations, the temperature is lowered by about $\frac{1}{2}$ during the very short span of time $w_p t \sim 3 \times 10^3$ [evaluated through Eq. (5)]. To obtain metastable glassy states in the MC simulations with large number of N (≥ 1458), a OCP would have to be quenched to a value of Γ much higher than 300–400.

[1] J.-P. Hansen and I. R. McDonald, *Theory of Simple Liquids*, 2nd ed. (Academic, London, 1986).

[2] See, for example, *Monte Carlo Methods in Statistical Physics*, edited by K. Binder (Springer-Verlag, Berlin, 1979).

[3] See, for example, G. Ciccotti, D. Frenkel, and I. R. McDonald, *Simulation of Liquids and Solids* (North-Holland, Amsterdam, 1987).

[4] B. J. Alder and T. E. Wainwright, J. Chem. Phys. **27**, 1208 (1957); **31**, 459 (1959).

[5] M. Baus and J.-P. Hansen, Phys. Rep. **59**, 1 (1980).

[6] S. Ichimaru, H. Iyetomi, and S. Tanaka, Phys. Rep. **149**, 91 (1987).

[7] H. M. Van Horn, in *Strongly Coupled Plasma Physics*, edited by S. Ichimaru (North-Holland, Amsterdam, 1990), p. 3; S. L. Shapiro and S. A. Teukolsky, *Black Holes, White Dwarfs, and Neutron Stars* (Wiley, New York, 1983).

[8] S. Ogata and S. Ichimaru, Astrophys. J. **361**, 511 (1990).

[9] S. Ichimaru and S. Tanaka, Phys. Rev. Lett. **56**, 2815 (1986); S. Ogata and S. Ichimaru, Phys. Rev. A **42**, 4867 (1990).

[10] S. G. Brush, H. L. Sahlin, and E. Teller, J. Chem. Phys. **45**, 2102 (1966).

[11] J.-P. Hansen, Phys. Rev. A **8**, 3096 (1973).

[12] W. L. Slattery, G. D. Doolen, and H. E. DeWitt, Phys. Rev. A **21**, 2087 (1980); **26**, 2255 (1982).

[13] S. Ogata and S. Ichimaru, Phys. Rev. A **36**, 5451 (1987).

[14] H. L. Helfer, R. L. McCrory, and H. M. Van Horn, J. Stat. Phys. **48**, 397 (1981).

[15] S. Ogata and S. Ichimaru, Phys. Rev. A **39**, 1333 (1989) (referred to as paper I).

[16] S. Ogata and S. Ichimaru, Phys. Rev. Lett. **62**, 2293 (1989).

[17] S. Ogata and S. Ichimaru, J. Phys. Soc. Jpn. **58**, 356 (1989).

[18] S. Ogata and S. Ichimaru, J. Phys. Soc. Jpn. **58**, 3049 (1989).

[19] N. Metropolis, A. W. Rosenbluth, M. N. Rosenbluth, A. H. Teller, and E. Teller, J. Chem. Phys. **21**, 1087 (1953).

[20] S. Ogata and S. Ichimaru, Phys. Rev. A **38**, 1457 (1988).

[21] P. J. Steinhardt, D. R. Nelson, and M. Ronchetti, Phys. Rev. B **28**, 784 (1983).

[22] See, for example, L. D. Landau and E. M. Lifshitz, *Quantum Mechanics*, 3rd. ed. (Pergamon, Oxford, 1976), p. 433.

[23] S. L. Gilbert, J. J. Bollinger, and D. J. Wineland, Phys. Rev. Lett. **60**, 2022 (1988).

[24] A. Rahman and J. P. Schiffer, Phys. Rev. Lett. **57**, 1133 (1986); J. P. Schiffer, **61**, 1843 (1988).

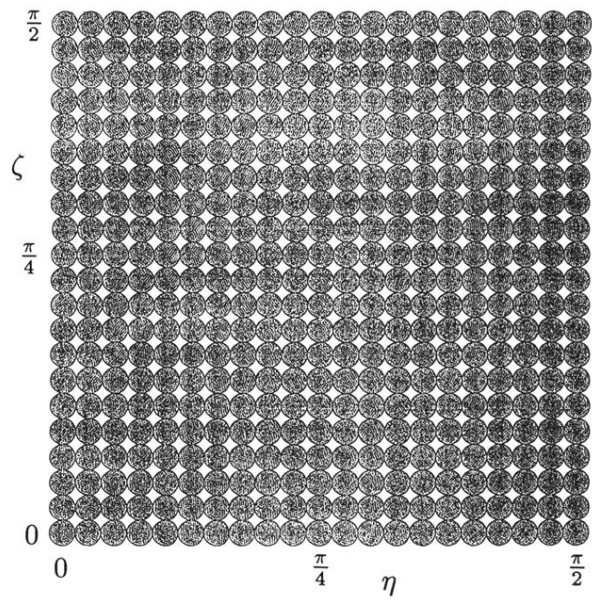[25] D. H. E. Dubin and T. M. O'Neil, Phys. Rev. Lett. **60**, 511 (1988).

FIG. 18. A collection of maps which are made by projecting particles onto the *y-z* plane with various rotation angles $(\zeta, \eta) = [(\pi/40)i, (\pi/40)j]$, $i,j = 0,1,...,20$.